Eur. Phys. J. Plus (2014) **129**: 248
DOI 10.1140/epjp/i2014-14248-2

THE EUROPEAN PHYSICAL JOURNAL PLUS

Regular Article

Effect of spatially variable magnetic field on ferrofluid flow and heat transfer considering constant heat flux boundary condition

Mohsen Sheikholeslami Kandelousi[a]

Department of Mechanical Engineering, Babol University of Technology, Babol, Islamic Republic of Iran

Received: 15 July 2014 / Revised: 17 October 2014
Published online: 18 November 2014 –

Abstract. Ferrofluid flow and heat transfer in the presence of an external variable magnetic field is studied. The inner cylinder is maintained at uniform heat flux and the outer cylinder has constant temperature. The Control Volume based Finite Element Method (CVFEM) is applied to solve the governing equations. Combined magnetohydrodynamic and ferrohydrodynamic effects have been taken into account. The effects of magnetic number, Hartmann number, Rayleigh number and nanoparticle volume fraction on hydrothermal behavior have been examined. Results show that the Nusselt number is an increasing function of Magnetic number, Rayleigh number and nanoparticle volume fraction while it is a decreasing function of the Hartmann number. Also, it can be concluded that the enhancement in heat transfer decreases with an increase in the Rayleigh number and magnetic number but it increases with an increase in the Hartmann number.

Nomenclature

B	Magnetic induction ($= \mu_0 H$)	*Greek symbols*	
C_p	Specific heat at constant pressure	ζ	Angle measured from the lower right plane
Ec	Eckert number ($= (\mu_f \alpha_f)/[(\rho C_P)_f \Delta T\, L^2]$)	α	Thermal diffusivity
En	Heat transfer enhancement	ϕ	Volume fraction
Gr_f	Grashof number	γ	Magnetic field strength at the source
H_x, H_y	Components of the magnetic field intensity	ε_1	Temperature number ($= T_1/\Delta T$)
H	The magnetic field strength	σ	Electrical conductivity
Ha	Hartmann number ($= \mu_0 H_0 L\sqrt{\sigma_f/\mu_f}$)	μ	Dynamic viscosity
Mn_F	Magnetic number arising from FHD ($= \mu_0 H_0^2 K' \Delta T\, L^2/(\mu_f \alpha_f)$)	μ_0	Magnetic permeability of vacuum ($= 4\pi \times 10^{-7}$ Tm/A)
M	Magnetization ($= K'\overline{H}(T_c' - T)$)	υ	Kinematic viscosity
Nu_{loc}	Local Nusselt number	ψ and Ψ	stream function and dimensionless stream function
Nu_{ave}	Average Nusselt number	Θ	dimensionless temperature
Pr	Prandtl number ($= \upsilon_f/\alpha_f$)	ρ	Fluid density
T	Fluid temperature	β	Thermal expansion coefficient
T_c'	Curie temperature	*Subscripts*	
u, v	Velocity components in the x-direction and y-direction	c	Cold
U, V	Dimensionless velocity components in the x-direction and y-direction	h	Hot
x, y	Space coordinates	nf	Nanofluid
X, Y	Dimensionless space coordinates	f	Base fluid

[a] e-mail: m_sh_3750@yahoo.com

r	Non-dimensional radial distance	s	Solid particles
k	Thermal conductivity	in	Inner
L	Gap between inner and outer boundary of the enclosure $L = r_{\text{out}} - r_{\text{in}}$	out	Outer
$\overrightarrow{g}$	Gravitational acceleration vector		
q''	Heat flux		
Ra	Rayleigh number ($= g\beta_f \Delta T L^3/\alpha_f \upsilon_f$)		

1 Introduction

The CVFEM uses the advantages of both finite volume and finite element methods for the simulation of multi-physics problems in complex geometries [1]. Sheikholeslami *et al.* [2] used CVFEM to simulate the effect of a magnetic field on natural convection in an inclined half-annulus enclosure filled with a Cu-water nanofluid. Their results indicated that the Hartmann number and the inclination angle of the enclosure can be considered as control parameters at a different Rayleigh number. This new method was applied for different kinds of problems [3–15].

Recently a wide research work has been done on the fluids dynamics in the presence of a magnetic field. The effect of the magnetic field on fluids is worth investigating due to its numerous applications in a wide range of fields. The study of the interaction of the magnetic field or the electromagnetic field on fluids has been documented, *e.g.*, in nuclear fusion, chemical engineering, medicine and transformer cooling. A magnetic nanofluid (ferrofluid) is a magnetic colloidal suspension consisting of a base liquid and magnetic nanoparticles with a size range of 5–15 nm in diameter coated with a surfactant layer. Ferrohydrodynamic and magnetohydrodynamic effects on the ferrofluid flow and the convective heat transfer was studied by Sheikholeslami and Ganji [16]. They proved that the magnetic number has a different effect on the Nusselt number compared to the Rayleigh number. The vortex dynamics behind various magnetic obstacles and characteristics of heat transfer were investigated by Zhang and Huang [17]. They found that the pressure drop penalty is not increasingly dependent on the interaction parameter. Jue [18] used the semi-implicit finite element method in order to simulate magnetic gradient and thermal buoyancy induced cavity ferrofluid flow. Their results showed that the flow strength increases with strengthening the magnetic field.

Azizian *et al.* [19] studied the effect of an external magnetic field on the convective heat transfer and pressure drop of magnetite nanofluids under laminar flow regime conditions. They showed that, based on the simulation results of magnetic field and magnetic force distribution, the mechanisms for heat transfer enhancement are postulated to be an accumulation of particles near the magnets (leading to higher thermal conductivity locally), and a formation of aggregates acting in enhancing momentum and energy transfer in the flow. Free convection of a ferrofluid in a cavity heated from below in the presence of an external magnetic field was studied by Sheikholeslami and Gorji [20]. They found that particles with a smaller size have a better ability to dissipate heat, and that a larger volume fraction would provide a stronger driving force which leads to an increase in the temperature profile. Numerical analysis of the heat transfer enhancement and fluid flow characteristics of a rotating cylinder under the influence of magnetic dipole in the backward facing step geometry was conducted by Selimefendigil and Oztop [21]. They found that the effect of the cylinder rotation on the local Nusselt number distribution is more pronounced at low Reynolds numbers. Nanjundappa *et al.* [22] studied the effect of magnetic-field–dependent (MFD) viscosity on the onset in a ferrofluid-saturated horizontal porous layer. They showed that the nonlinearity of fluid magnetization has no influence on the stability of the system. Also other authors used different methods to simulate nanofluid flow and heat transfer [23–62].

The main purpose of the present work is to study the effects of MHD and FHD on ferrofluid flow and heat transfer. CVFEM is applied to solve this problem. The numerical investigation is carried out for different governing parameters such as the Rayleigh number, nanoparticle volume fraction, magnetic number and Hartmann number.

2 Geometry definition and boundary conditions

The physical model along with the important geometrical parameters and the mesh of the enclosure used in the present CVFEM program are shown in fig. 1. The two horizontal walls are thermally isolated; the outer cylinder is maintained at constant cold temperature T_c, whereas the inner circular wall is under constant heat flux. To assess the shape of the inner circular and of the outer rectangular boundary, which consists of the right and top walls, a supper elliptic function can be used as follows:

$$\left(\frac{X}{a}\right)^{2n} + \left(\frac{Y}{b}\right)^{2n} = 1. \tag{1}$$

When $a = b$ and $n = 1$ the geometry becomes a circle. As n increases from 1 the geometry approaches a rectangle for $a \neq b$ and a square for $a = b$. In this study, $r_{\text{in}}/r_{\text{out}} = 0.6$.

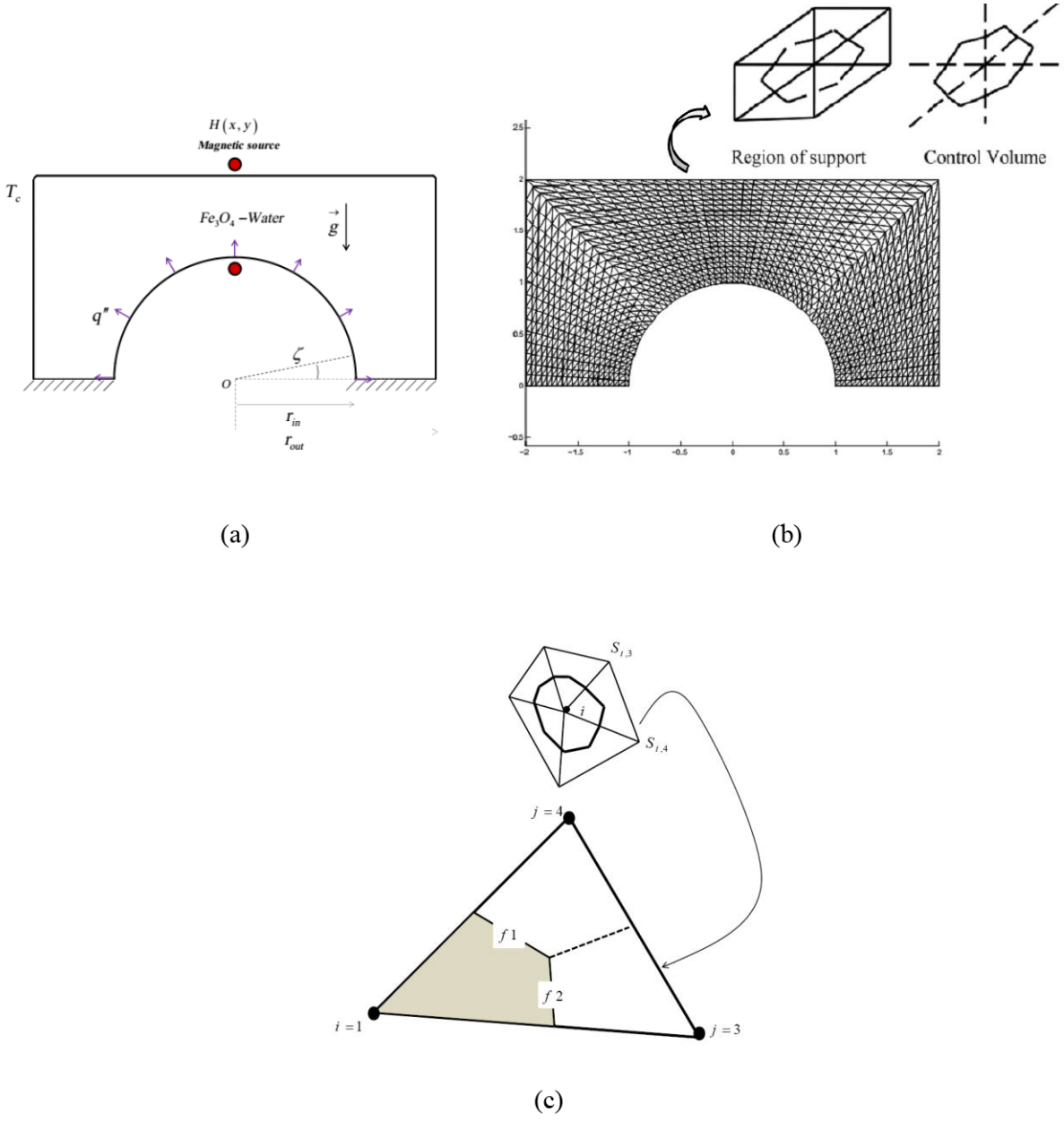

Fig. 1. (a) Geometry and the boundary conditions; (b) the mesh of enclosure considered in this work; (c) a sample triangular element and its corresponding control volume.

For the expression of the magnetic field strength it can be considered that two magnetic sources are located at the points $(\overline{a_1}, \overline{b_1})$ and $(\overline{a}_2, \overline{b_2})$. The components of the magnetic field intensity $(\overline{H_x}, \overline{H_y})$ and the magnetic field strength $(\overline{H})$ can be considered as [16]

$$\overline{H_x} = \frac{\gamma}{2\pi}\frac{1}{(x-\overline{a_1})^2+(y-\overline{b_1})^2}(y-\overline{b_1}) - \frac{\gamma}{2\pi}\frac{1}{(x-\overline{a_2})^2+(y-\overline{b_2})^2}(y-\overline{b_2}), \tag{2}$$

$$\overline{H_y} = -\frac{\gamma}{2\pi}\frac{1}{(x-\overline{a_1})^2+(y-\overline{b_1})^2}(x-\overline{a_1}) - \frac{\gamma}{2\pi}\frac{1}{(x-\overline{a_2})^2+(y-\overline{b_2})^2}(x-\overline{a_2}), \tag{3}$$

$$\overline{H} = \sqrt{\overline{H}_x^2 + \overline{H}_y^2}, \tag{4}$$

where γ the magnetic field strength at the source (of the wire). The contours of the magnetic field strength are shown in fig. 2. In this study, the magnetic source is located at $(\overline{a_1} = 1.05\text{cols}, \overline{b_1} = 0.5\text{rows})$ and $(\overline{a}_2 = -0.05\text{cols}, \overline{b_2} = 0.5\text{rows})$.

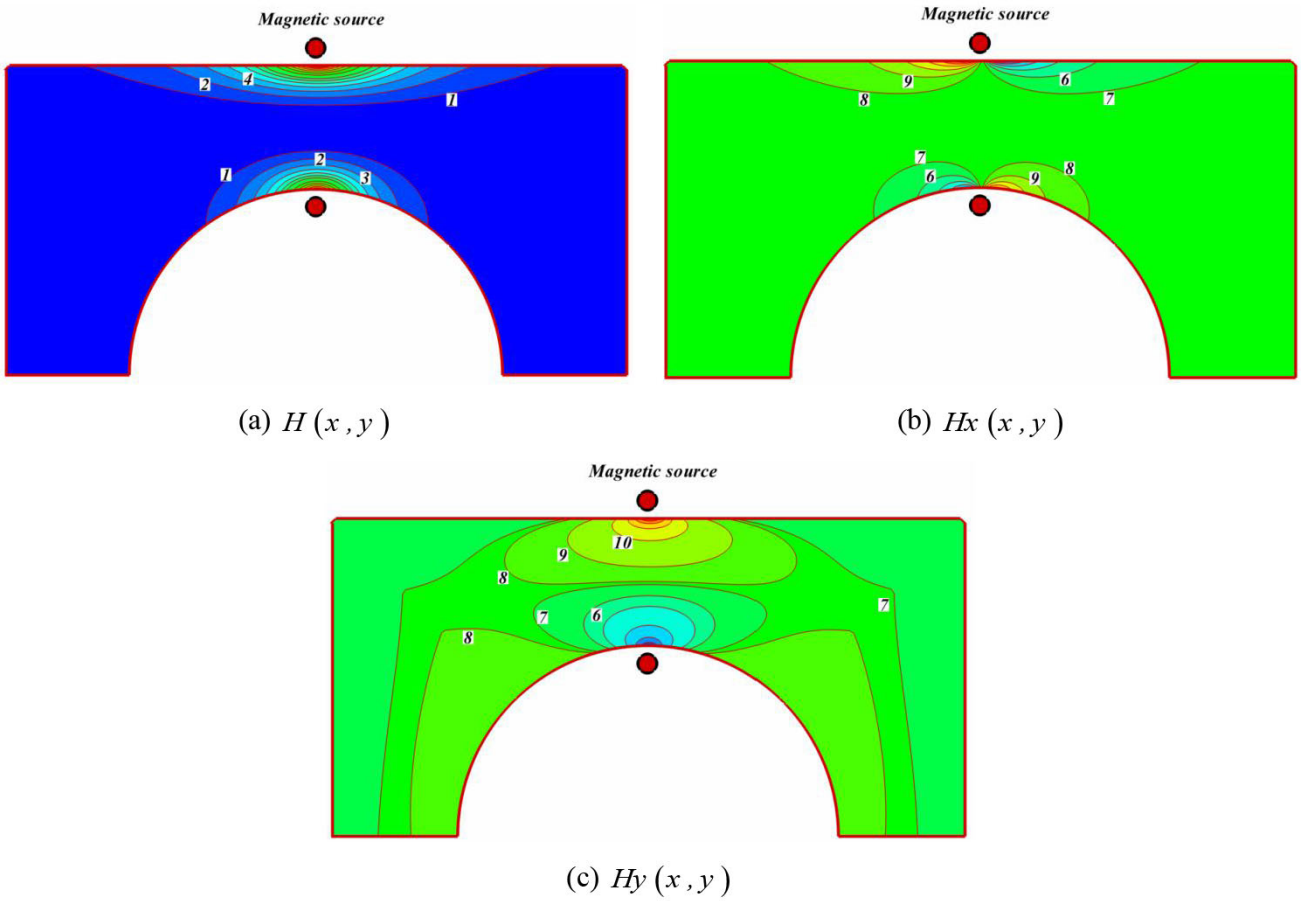

(a) $H(x, y)$ (b) $Hx(x, y)$

(c) $Hy(x, y)$

Fig. 2. Contours of the (a) magnetic field strength H; (b) magnetic field intensity component in the x-direction Hx; (c) magnetic field intensity component in the y-direction Hy.

3 Mathematical modeling and numerical procedure

3.1 Problem formulation

The flow is two-dimensional, laminar and incompressible. The magnetic Reynolds number is assumed to be small so that the induced magnetic field can be neglected compared to the applied magnetic field. The flow is considered to be steady, two-dimensional and laminar. Using the Boussinesq approximation, the governing equations of heat transfer and fluid flow for nanofluid can be obtained as follows:

$$\frac{\partial u}{\partial x} + \frac{\partial v}{\partial y} = 0, \tag{5}$$

$$\rho_{nf}\left(u\frac{\partial u}{\partial x} + v\frac{\partial u}{\partial y}\right) = -\frac{\partial P}{\partial x} + \mu_{nf}\left(\frac{\partial^2 u}{\partial x^2} + \frac{\partial^2 u}{\partial y^2}\right) + \mu_0 M\frac{\partial \overline{H}}{\partial x} - \sigma_{nf}B_y^2 u + \sigma_{nf}B_x B_y v, \tag{6}$$

$$\begin{aligned}\rho_{nf}\left(u\frac{\partial v}{\partial x} + v\frac{\partial v}{\partial y}\right) = &-\frac{\partial P}{\partial y} + \mu_{nf}\left(\frac{\partial^2 v}{\partial x^2} + \frac{\partial^2 v}{\partial y^2}\right) + \mu_0 M\frac{\partial \overline{H}}{\partial y} \\ &-\sigma_{nf}B_x^2 v + \sigma_{nf}B_x B_y u + \rho_{nf}\beta_{nf}g(T - T_c),\end{aligned} \tag{7}$$

$$\begin{aligned}(\rho C_p)_{nf}\left(u\frac{\partial T}{\partial x} + v\frac{\partial T}{\partial y}\right) = &\, k_{nf}\left(\frac{\partial^2 T}{\partial x^2} + \frac{\partial^2 T}{\partial y^2}\right) + \sigma_{nf}(uB_y - vB_x)^2 - \mu_0 T\frac{\partial M}{\partial T}\left(u\frac{\partial \overline{H}}{\partial x} + v\frac{\partial \overline{H}}{\partial y}\right) \\ &+\mu_{nf}\left\{2\left(\frac{\partial u}{\partial x}\right)^2 + 2\left(\frac{\partial v}{\partial x}\right)^2 + \left(\frac{\partial u}{\partial x} + \frac{\partial v}{\partial y}\right)^2\right\}.\end{aligned} \tag{8}$$

The terms $\mu_0 M \frac{\partial \overline{H}}{\partial x}$ and $\mu_0 M \frac{\partial \overline{H}}{\partial y}$ in (6) and (7), respectively, represent the components of magnetic force per unit volume, and depend on the existence of the magnetic gradient on the corresponding x and y directions. These two terms are well known from FHD, which is the so-called Kelvin force. The terms $-\sigma_{nf} B_y^2 u + \sigma_{nf} B_x B_y v$ and $-\sigma_{nf} B_x^2 v + \sigma_{nf} B_x B_y u$ appearing in (6) and (7), respectively, represent the Lorentz force per unit volume towards the x and y directions and arise due to the electrical conductivity of the fluid. These two terms are known in MHD. The principles of MHD and FHD are combined in the mathematical model presented in [16] and the above-mentioned terms arise together in the governing equations (6) and (7). The term $\mu_0 T \frac{\partial M}{\partial T}\left(u \frac{\partial \overline{H}}{\partial x} + v \frac{\partial \overline{H}}{\partial y}\right)$ in eq. (8) represents the thermal power per unit volume due to the magnetocaloric effect. Also, the term $\sigma_{nf}(uB_y - vB_x)^2$ in (8) represents the Joule heating. For the variation of the magnetization M, with the magnetic field intensity $\overline{H}$ and temperature T, the following relation derived experimentally in [63] is considered:

$$M = K' \overline{H}(T_c' - T), \tag{9}$$

where K' is a constant and T_c' is the Curie temperature.

In the above equations, μ_0 is the magnetic permeability of vacuum ($4\pi \times 10^{-7}$ Tm/A), $\overline{H}$ is the magnetic field strength, $\overline{B}$ is the magnetic induction ($\overline{B} = \mu_0 \overline{H}$) and the bar above the quantities denotes that they are dimensional. The effective density (ρ_{nf}) and heat capacitance $(\rho C_p)_{nf}$ of the nanofluid are defined as [12]

$$\rho_{nf} = \rho_f(1-\phi) + \rho_s \phi, \tag{10}$$

$$(\rho C_p)_{nf} = (\rho C_p)_f (1-\phi) + (\rho C_p)_s \phi, \tag{11}$$

where ϕ is the solid volume fraction of nanoparticles. Thermal diffusivity of the nanofluid is

$$\alpha_{nf} = \frac{k_{nf}}{(\rho C_p)_{nf}} \tag{12}$$

and the thermal expansion coefficient of the nanofluid can be determined as

$$\beta_{nf} = \beta_f(1-\phi) + \beta_s \phi. \tag{13}$$

The dynamic viscosity of the nanofluid given by Brinkman [12] is

$$\mu_{nf} = \frac{\mu_f}{(1-\phi)^{2.5}}. \tag{14}$$

The effective thermal conductivity of the nanofluid can be approximated by the Maxwell-Garnetts (MG) model as [12]

$$\frac{k_{nf}}{k_f} = \frac{k_s + 2k_f - 2\phi(k_f - k_s)}{k_s + 2k_f + \phi(k_f - k_s)} \tag{15}$$

and the effective electrical conductivity of nanofluid was presented by Maxwell [12] as follows:

$$\frac{\sigma_{nf}}{\sigma_f} = 1 + \frac{3\left(\frac{\sigma_s}{\sigma_f} - 1\right)\phi}{\left(\frac{\sigma_s}{\sigma_f} + 2\right) - \left(\frac{\sigma_s}{\sigma_f} - 1\right)\phi}. \tag{16}$$

The stream function and vorticity are defined as

$$u = \frac{\partial \psi}{\partial y}, \qquad v = -\frac{\partial \psi}{\partial x}, \qquad \omega = \frac{\partial v}{\partial x} - \frac{\partial u}{\partial y}. \tag{17}$$

The stream function satisfies the continuity equation (4). The vorticity equation is obtained by eliminating the pressure between the two momentum equations, *i.e.* by taking the y-derivative of eq. (6) and subtracting from it the x-derivative of eq. (5). By introducing the following non-dimensional variables,

$$X = \frac{x}{L}, \qquad Y = \frac{y}{L}, \qquad \Omega = \frac{\omega L^2}{\alpha_f}, \qquad \Psi = \frac{\psi}{\alpha_f}, \qquad \Theta = \frac{T - T_c}{(q'' L/k_f)},$$

$$U = \frac{uL}{\alpha_f}, \qquad V = \frac{vL}{\alpha_f}, \qquad H = \frac{\overline{H}}{\overline{H_0}}, \qquad H_x = \frac{\overline{H_x}}{\overline{H_0}}, \qquad H_y = \frac{\overline{H_y}}{\overline{H_0}}, \tag{18}$$

Table 1. Thermophysical properties of water and nanoparticles [64].

	ρ (kg/m^3)	C_p (j/kgk)	k (W/m·k)	$\beta \times 10^5$ (K^{-1})	σ $(\Omega \cdot m)^{-1}$
Pure water	997.1	4179	0.613	21	0.05
Fe_3O_4	5200	670	6	1.3	25000

where, in eq. (18), $\overline{H_0} = \overline{H}(\overline{a}, 0) = \frac{\gamma}{2\pi|b|}$ and $L = r_{\text{out}} - r_{\text{in}} = r_{\text{in}}$. Using the dimensionless parameters, the equations now become

$$\begin{aligned}\frac{\partial \Psi}{\partial Y}\frac{\partial \Omega}{\partial X} - \frac{\partial \Psi}{\partial X}\frac{\partial \Omega}{\partial Y} &= Pr\left[\frac{\mu_{nf}/\mu_f}{\rho_{nf}/\rho_f}\right]\left(\frac{\partial^2 \Omega}{\partial X^2} + \frac{\partial^2 \Omega}{\partial Y^2}\right) + RaPr\left[\frac{\beta_{nf}}{\beta_f}\right]\left(\frac{\partial \Theta}{\partial X}\right)\\ &+ Mn_F Pr\left(\frac{\rho_f}{\rho_{nf}}\right)\left\{\frac{\partial H}{\partial X}\frac{\partial \Theta}{\partial Y} - \frac{\partial H}{\partial Y}\frac{\partial \Theta}{\partial X}\right\} - Ha^2 Pr\left[\frac{\sigma_{nf}/\sigma_f}{\rho_{nf}/\rho_f}\right]\\ &\times\left\{\frac{\partial V}{\partial X}H_x^2 + V\left(2H_x\frac{\partial H_x}{\partial X}\right) - \frac{\partial U}{\partial X}H_xH_y - U\frac{\partial H_x}{\partial X}H_y - U\frac{\partial H_y}{\partial X}H_x - \frac{\partial U}{\partial Y}H_y^2\right.\\ &\left.- U\left(2H_y\frac{\partial H_y}{\partial Y}\right) + \frac{\partial V}{\partial Y}H_xH_y + V\frac{\partial H_x}{\partial Y}H_y + V\frac{\partial H_y}{\partial Y}H_x\right\}, \end{aligned} \tag{19}$$

$$\begin{aligned}\frac{\partial \Psi}{\partial Y}\frac{\partial \Theta}{\partial X} - \frac{\partial \Psi}{\partial X}\frac{\partial \Theta}{\partial Y} &= \left[\frac{\frac{k_{nf}}{k_f}}{\frac{(\rho C_P)_{nf}}{(\rho C_P)_f}}\right]\left(\frac{\partial^2 \Theta}{\partial X^2} + \frac{\partial^2 \Theta}{\partial Y^2}\right) + Ha^2 Ec\left[\frac{\frac{\sigma_{nf}}{\sigma_f}}{\frac{(\rho C_P)_{nf}}{(\rho C_P)_f}}\right]\{UH_y - VH_x\}^2\\ &+ Mn_F Ec\frac{(\rho C_P)_f}{(\rho C_P)_{nf}}\left\{U\frac{\partial H}{\partial X} + V\frac{\partial H}{\partial Y}\right\}H(\varepsilon_1 + \Theta)\\ &+ Ec\left[\frac{\frac{\mu_{nf}}{\mu_f}}{\frac{(\rho C_P)_{nf}}{(\rho C_P)_f}}\right]\left\{2\left(\frac{\partial U}{\partial X}\right)^2 + 2\left(\frac{\partial V}{\partial X}\right)^2 + \left(\frac{\partial U}{\partial X} + \frac{\partial V}{\partial Y}\right)^2\right\}, \end{aligned} \tag{20}$$

$$\frac{\partial^2 \Psi}{\partial X^2} + \frac{\partial^2 \Psi}{\partial Y^2} = -\Omega, \tag{21}$$

where $Ra_f = g\beta_f L^4 q''/(k_f \alpha_f \nu_f)$, $Pr_f = \upsilon_f/\alpha_f$, $Ha = LB_x\sqrt{\sigma_f/\mu_f}$, $\varepsilon_1 = T_1/\Delta T$, $\Delta T = (q''L/k_f)$, $Ec = (\mu_f \alpha_f)/[(\rho C_P)_f \Delta T L^2]$ and $Mn_F = \mu_0 H_0^2 K' \Delta T L^2/(\mu_f \alpha_f)$ are the Rayleigh number, Prandtl number, Hartmann number arising from MHD, temperature number, Eckert number and magnetic number arising from FHD the for the base fluid, respectively. The thermophysical properties of the nanofluid are given in table 1 [64]. The boundary conditions, as shown in fig. 1, are

$$\begin{aligned}\frac{\partial \Theta}{\partial n} &= -1 \quad \text{on the inner circular boundary,}\\ \Theta &= 0.0 \quad \text{on the outer circular boundary,}\\ \Psi &= 0.0 \quad \text{on all solid boundaries.}\end{aligned} \tag{22}$$

The values of vorticity on the boundary of the enclosure can be obtained using the stream function formulation and the known velocity conditions during the iterative solution procedure.

The local Nusselt number of the nanofluid along the inner wall can be expressed as

$$Nu_{\text{local}} = \left(\frac{k_{nf}}{k_f}\right)\frac{1}{\theta}\bigg|_{\text{inner wall}}, \tag{23}$$

where r is the radial direction. The average Nusselt number on the hot circular wall is evaluated as

$$Nu_{\text{ave}} = \frac{1}{\gamma}\int_0^{\gamma} Nu_{\text{loc}}(\zeta)\mathrm{d}\zeta. \tag{24}$$

To estimate the enhancement of heat transfer between the case of $\phi = 0.04$ and the pure fluid (base fluid) case, the heat transfer enhancement is defined as

$$En = \frac{Nu(\phi = 0.04) - Nu(\text{basefluid})}{Nu(\text{basefluid})} \times 100. \tag{25}$$

Table 2. Comparison of the average Nusselt number, Nu_{ave}, along the hot wall for different grid resolutions at $Ra = 10^5$, $\phi = 0.04$, $Mn_F = 100$, $Ha = 10$, $Ec = 10^{-6}$, $\varepsilon_1 = 0$ and $Pr = 6.8$.

31×91	41×121	51×151	61×181	71×211	81×241	91×271	101×301
5.55056	5.490303	5.454067	5.431622	5.415271	5.403593	5.401344	5.399344

Table 3. Comparison of the present results with previous works for different Rayleigh numbers when $Pr = 0.7$.

Ra	Present	Khanafer *et al.* [65]	De Vahl Davis [66]
10^3	1.1432	1.118	1.118
10^4	2.2749	2.245	2.243
10^5	4.5199	4.522	4.519

3.2 Numerical procedure

A control volume finite element method is used in this work. The building block of the discretization is the triangular element and the values of variables are approximated with linear interpolation within the elements. The control volumes are created by joining the center of each element in the support to the mid-points of the element sides that pass through the central node i, which creates a close polygonal control volume (see fig. 1(c)). The set of governing equations is integrated over the control volume with the use of linear interpolation inside the finite element and the obtained algebretic equations are solved by the Gauss-Seidel method. A FORTRAN code is developed to solve the present problem using a structured mesh of linear triangular. The details of this method are mentioned in [12].

4 Grid testing and code validation

A mesh testing procedure was conducted to guarantee the grid independency of the present solution. Various mesh combinations were explored for the case of $Ra = 10^5$, $\phi = 0.04$, $Mn_F = 100$, $Ha = 10$, $Ec = 10^{-6}$, $\varepsilon_1 = 0$ and $Pr = 6.8$, as shown in table 2. The present code was tested for grid independence by calculating the average Nusselt number on the inner hot wall. In harmony with this, it was found that a grid size of 71×211 ensures a grid-independent solution. The convergence criterion for the termination of all computations is

$$\max_{\text{grid}} |\Gamma^{n+1} - \Gamma^n| \leq 10^{-7}, \tag{26}$$

where n is the iteration number and Γ stands for the independent variables (Ω, Ψ, Θ). To validate the present study the results obtained using the CVFEM code are compared for $Pr = 0.7$ with other works reported in [65] and [66] as can be seen in table 3. Moreover, the code was compared with the work of Khanafer *et al.* [65] in fig. 3 for natural convection in an enclosure filled with Cu-water nanofluid. These comparisons illustrate an excellent agreement between the present calculations and the previous works.

5 Results and discussion

Fe_3O_4-water flow and heat transfer in the presence of a variable external magnetic field is studied numerically using the control volume based finite element method. Constant heat flux boundary condition is considered for inner wall. The thermophysical properties of Fe_3O_4 nanoparticles and based fluid (water) are shown in table 1 [64]. Calculations are made for various values of volume fraction of nanoparticles ($\phi = 0\%$ and 4%), Rayleigh numbers ($Ra = 10^3, 10^4$ and 10^5), magnetic number arising from FHD ($Mn_F = 0$, 20, 60 and 100) and Hartmann number arising from MHD ($Ha = 0$, 5 and 10). In all calculations, the Prandtl number (Pr), temperature number (ε_1) and Eckert number (Ec) are set to 6.8, 0.0 and 10^{-6}, respectively.

Figure 4 shows the comparison of the isotherms and streamlines between nanofluid and pure fluid. The velocity components of the nanofluid are increased because of an increase in the energy transport in the fluid with the increase in the volume fraction. Thus, the absolute values of stream functions indicate that the strength of flow increases with increasing the volume fraction of the nanofluid. Also, it can be seen that the thermal boundary layer thickness around the hot wall decreases with an increase in the nanoparticle volume fraction.

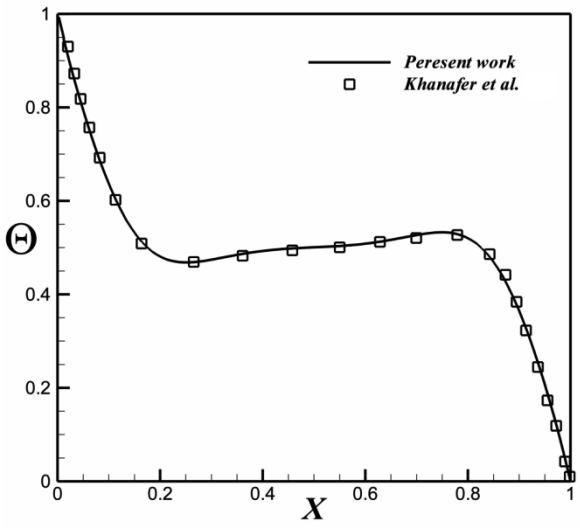

Fig. 3. Comparison of the average Nusselt number between the present results and numerical results by Khanafer *et al.* [65]; $Gr = 10^4$, $\phi = 0.1$ and $Pr = 6.8$ (*Cu-water*).

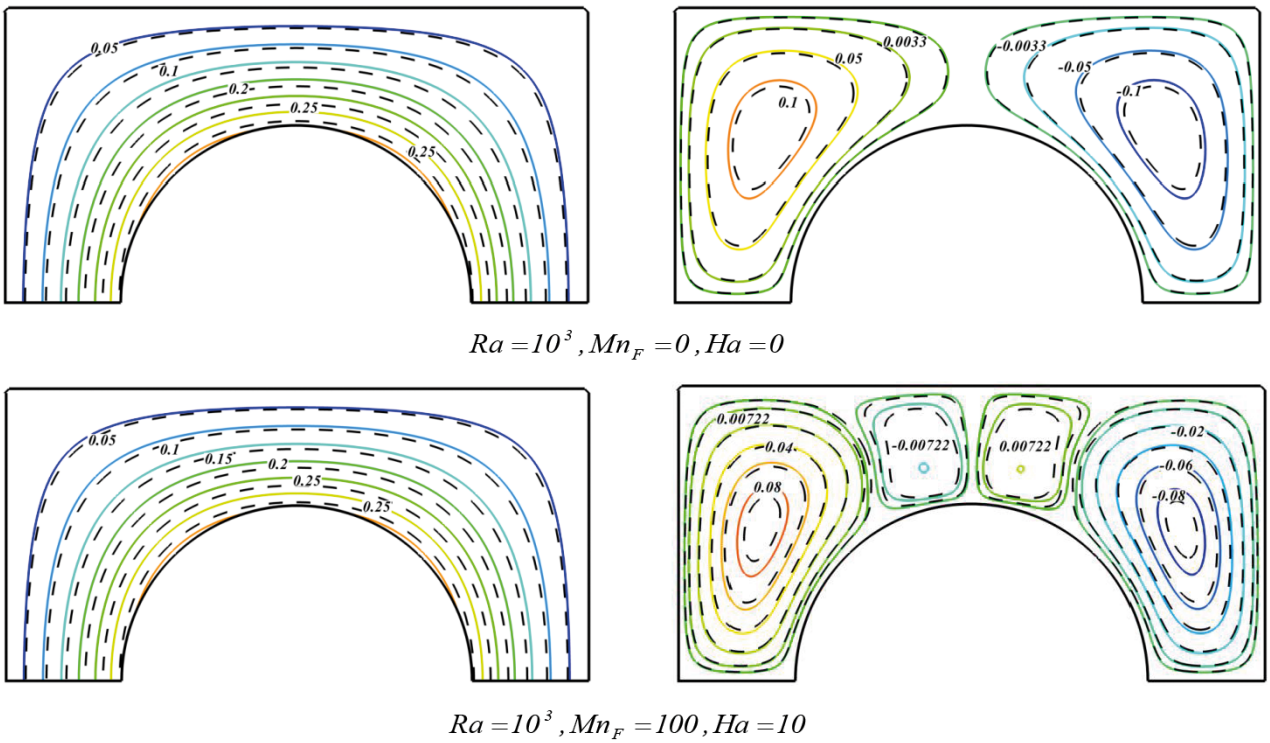

Fig. 4. Comparison of the isotherms and streamlines between nanofluid ($\phi = 0.04$) (− − −) and pure fluid ($\phi = 0$) (—) when $Pr = 6.8$.

Figure 5 depicts the effects of the Rayleigh number, Hartmann number and magnetic number on isotherms and streamlines. The absolut value of the stream function increases with an increase in the Rayleigh number, while it decreases with an increase in Hartmann number and magnetic number. When $Ra = 10^3$, the heat transfer in the enclosure is mainly dominated by the conduction mode. At $Mn_F = 0$, $Ha = 0$, the streamlines show one rotating eddy.

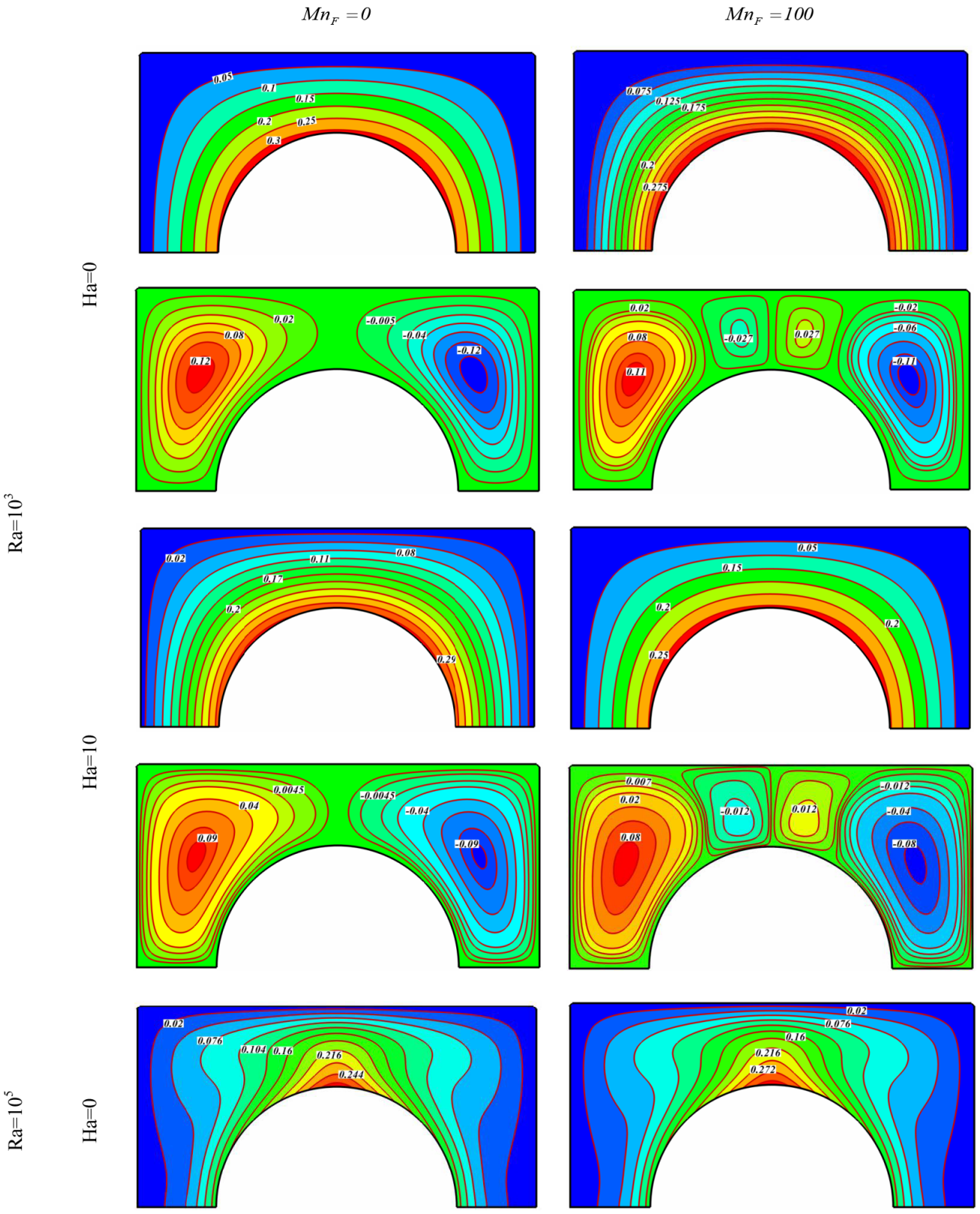

Fig. 5. Isotherms (left) and streamlines (right) contours for different values of Rayleigh number, Hartmann number and magnetic number when $Pr = 6.8$, $\phi = 0.04$.

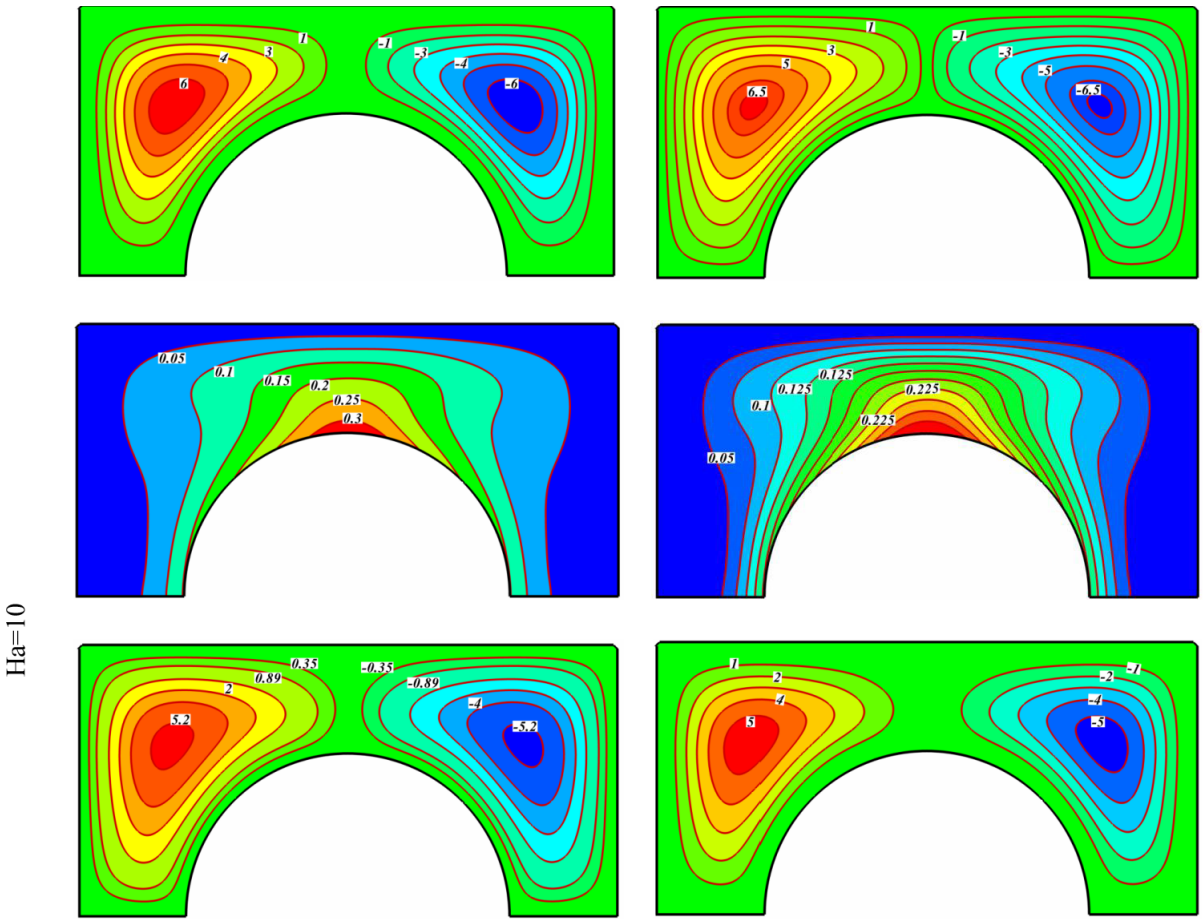

Fig. 5. Continued.

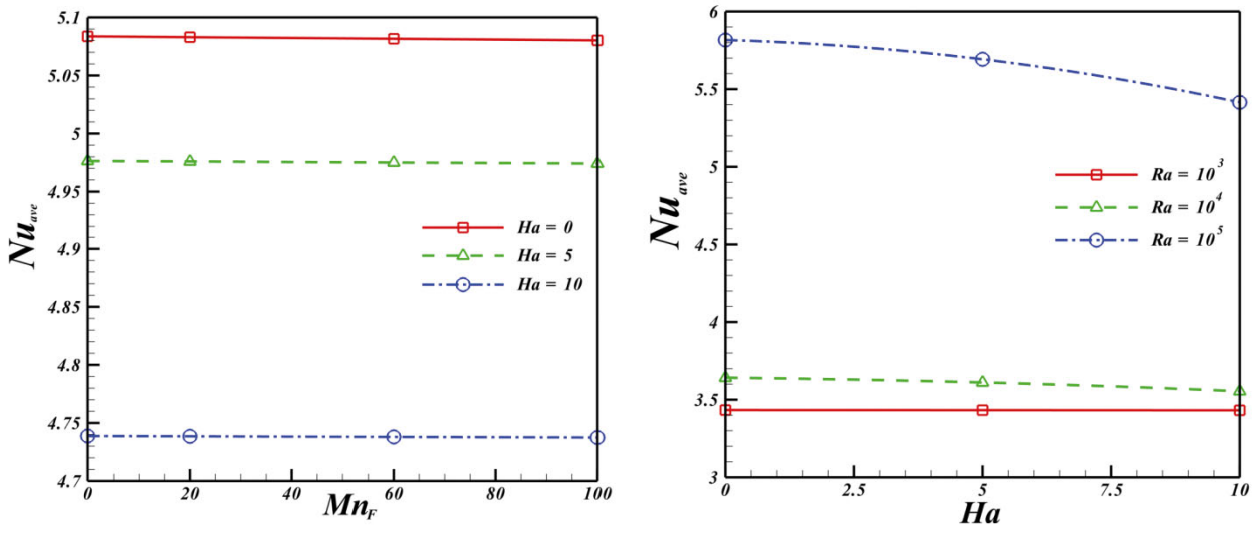

(a) $Ra = 10^5$ (b) $Mn_F = 100$

Fig. 6. Effects of magnetic parameter, Hartmann number and Rayleigh number on the average Nusselt number Nu_{ave} along the hot wall when $Pr = 6.8$, $\phi = 0.04$.

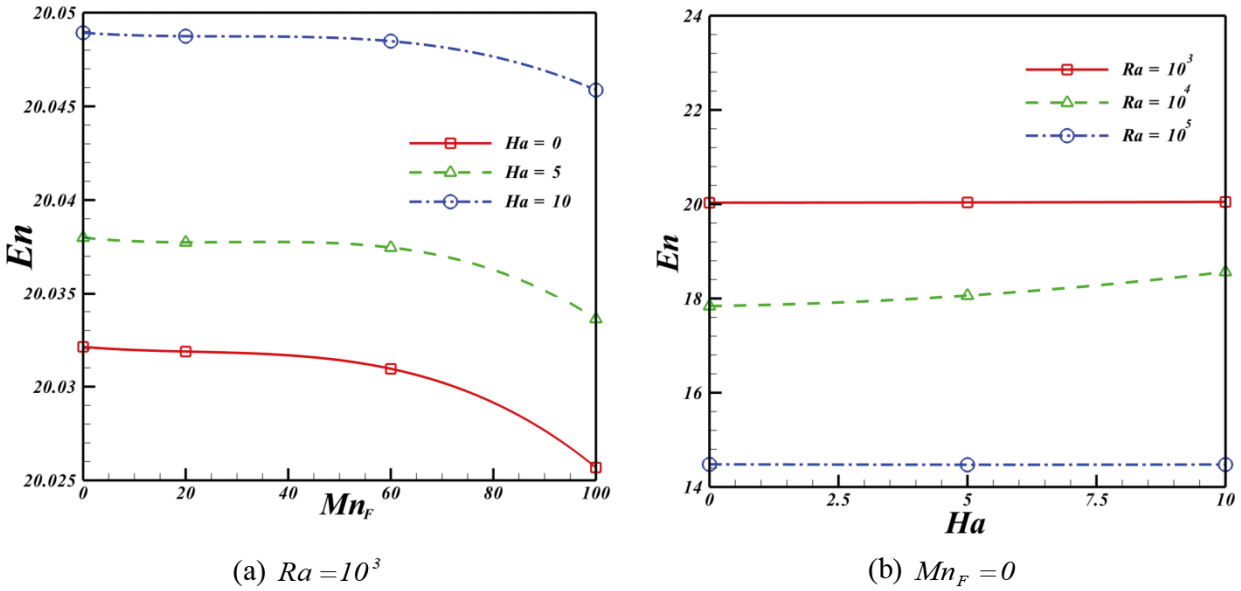

(a) $Ra = 10^3$ (b) $Mn_F = 0$

Fig. 7. Effects of magnetic number, Rayleigh number and Hartmann number on heat transfer enhancement when $Pr = 6.8$.

When the magnetic parameter increases, another vortex appears near the centerline, which rotates in reverse direction in comparison to the primary vortex. The Lorentz force has no significant effect on isotherm and streamline in this Rayleigh number. As the Rayleigh number increases up to 10^5, the role of convection in heat transfer becomes more significant and consequently the thermal boundary layer on the surface of the inner wall becomes thinner. In addition, a plume starts to appear on the top of the inner circular wall. The effect of the magnetic field on the hydrothermal behavior is more pronounced for low Rayleigh numbers.

Figure 6 shows the effects of the magnetic parameter, Hartmann number and Rayleigh number on average Nusselt number along the inner wall. The Nusselt number increases with an increase in Rayleigh number and magnetic parameter, while it decreases with an increase in the Hartmann number. The effects of magnetic number, Rayleigh number and Hartmann number on the heat transfer enhancement are shown in fig. 7. Heat transfer enhancement is an increasing function of the Hartmann number, while it is a decreasing function of the magnetic number and Rayleigh number. The effect of nanoparticles is more pronounced at low Rayleigh numbers than at high Rayleigh numbers because of the greater enhancement rate. This observation can be explained by noting that at low Rayleigh numbers the heat transfer is dominant by conduction.

6 Conclusions

Natural convection heat transfer in an enclosure filled with a Fe_3O_4-water nanofluid is investigated in the presence of an external magnetic field. Combined MHD and FHD effects are considered. CVFEM is used to solve the governing equations. The effects of the Rayleigh number, nanoparticle volume fraction, magnetic number and Hartmann number on the flow and heat transfer characteristics have been examined. Results show that the Nusselt number increases with an increase in magnetic number, Rayleigh number and nanoparticle volume fraction, while it decreases with an increase in the Hartmann number. Heat transfer enhancement increases with an increase in the Hartmann number but it decreases with an increase in Rayleigh number and Magnetic number.

References

1. B.R. Baliga, S.V. Patankar, Numer. Heat Transfer **6**, 245 (1983).
2. M. Sheikholeslami, M. Gorji-Bandpy, D.D. Ganji, Soheil Soleimani, Adv. Powder Technol. **24**, 980 (2013).
3. Mohsen Sheikholeslami, Davood Domiri Ganji, Mohammad Mehdi Rashidi, J. Taiwan Inst. Chem. Eng. (2014) http://dx.doi.org/10.1016/j.jtice.2014.09.026.
4. M. Sheikholeslami, M. Gorji-Bandpy, D.D. Ganji, Soheil Soleimani, Trans. Mech. Eng. **38**, 217 (2014).
5. M. Sheikholeslami, M. Gorji-Bandpy, D.D. Ganji, P. Rana, Soheil Soleimani, Comput. Fluids **94**, 147 (2014).
6. M. Sheikholeslami, M. Gorji-Bandpy, D.D. Ganji, Soheil Soleimani, J. Mol. Liq. **194**, 179 (2014).
7. M. Sheikholeslami, M. Gorji-Bandpy, D.D. Ganji, Soheil Soleimani, J. Mol. Liq. **193**, 174 (2014).

8. M. Sheikholeslami, M. Gorji-Bandpy, Soheil Soleimani, Int. Commun. Heat Mass Transfer **47**, 73 (2013).
9. M. Sheikholeslami, M. Gorji Bandpy, R. Ellahi, Mohsan Hassan, Soheil Soleimani, J. Magn. Magn. Mater. **349**, 188 (2014).
10. M. Sheikholeslami, M. Gorji-Bandpy, D.D. Ganji, Soheil Soleimani, J. Taiwan Inst. Chem. Eng. **45**, 40 (2014).
11. M. Sheikholeslami, I. Hashim, Soheil Soleimani, Math. Prob. Eng. **2013**, 831725 (2013).
12. M. Sheikholeslami, M. Gorji-Bandpy, D.D. Ganji, Soheil Soleimani, Adv. Powder Technol. **24**, 980 (2013).
13. M. Sheikholeslami, M. Gorji-Bandpy, D.D. Ganji, Soheil Soleimani, Neural Comput. Appl. **24**, 873 (2014).
14. M. Sheikholeslami, M. Gorji-Bandpy, D.D. Ganji, Soheil Soleimani, S.M. Seyyedi, Int. Commun. Heat Mass Transfer **39**, 1435 (2012).
15. Soheil Soleimani, M. Sheikholeslami, D.D. Ganji, M. Gorji-Bandpay, Int. Commun. Heat Mass Transfer **39**, 565 (2012).
16. Mohsen Sheikholeslami, Davood Domiri Ganji, Energy **75**, 400 (2014).
17. Xidong Zhang, Hulin Huang, Int. Commun. Heat Mass Transfer **51**, 31 (2014).
18. Tswen-Chyuan Jue, Int. Commun. Heat Mass Transfer **33**, 846 (2006).
19. R. Azizian, E. Doroodchi, T. McKrell, J. Buongiorno, L.W. Hu, B. Moghtaderi, Int. J. Heat Mass Transfer **68**, 94 (2014).
20. Mohsen Sheikholeslami, Mofid Gorji-Bandpy, Powder Technol. **256**, 490 (2014).
21. Fatih Selimefendigil, Hakan F. Oztop, Int. J. Heat Mass Transfer **71**, 142 (2014).
22. C.E. Nanjundappa, I.S. Shivakumara, M. Ravisha, Int. Commun. Heat Mass Transfer **37**, 1246 (2010).
23. Mohsen Sheikholeslami Kandelousi, Phys. Lett. A **378**, 3331 (2014).
24. Mohsen Sheikholeslami, Davood Domiri Ganji, Physica A **417**, 273 (2014).
25. Mohsen Sheikholeslami, Mofid Gorji-Bandpy, Kuppalapalle Vajravelu, Int. J. Heat Mass Transfer **80**, 16 (2015).
26. M. Sheikholeslami, J Braz. Soc. Mech. Sci. Eng. (2014) DOI: 10.1007/s40430-014-0242-z.
27. M. Sheikholeslami, M. Gorji-Bandpy, S.M. Seyyedi, D.D. Ganji, Houman B. Rokni, Soheil Soleimani, Powder Technol. **247**, 87 (2013).
28. W.A. Khan, O.D. Makinde, Int. J. Therm. Sci. **81**, 118 (2014).
29. W.A. Khan, O.D. Makinde, Z.H. Khan, Int. J. Heat Mass Transfer **74**, 285 (2014).
30. Winifred Nduku Mutuku, Oluwole Daniel Makinde, Comput. Fluids **95**, 88 (2014).
31. O.D. Makinde, A. Aziz, Int. J. Therm. Sci. **50**, 1326 (2011).
32. M. Sheikholeslami, M. Gorji-Bandpy, D.D. Ganji, Sci. Iran., Trans. B: Mech. Eng. **20**, 1241 (2013).
33. M. Sheikholeslami, M. Gorji-Bandpy, G. Domairry, Appl. Math. Mech. **34**, 1 (2013).
34. M. Sheikholeslami, D.D. Ganji, Powder Technol. **235**, 873 (2013).
35. M. Sheikholeslami, M. Gorji-Bandpay, D.D. Ganji, Int. Commun. Heat Mass Transfer **39**, 978 (2012).
36. Mohsen Sheikholeslami, Davood Domiri Ganji, M. Younus Javed, R. Ellahi, J. Magn. Magn. Mater. **374**, 36 (2015).
37. Mohsen Sheikholeslami, Shirley Abelman, Davood Domiri Ganji, Int. J. Heat Mass Transfer **79**, 212 (2014).
38. Mohsen Sheikholeslami, Davood Domiri Ganji, J Braz. Soc. Mech. Sci. Eng. (2014) DOI: 10.1007/s40430-014-0228-x.
39. Wubshet Ibrahim, O.D. Makinde, Comput. Fluids **86**, 433 (2013).
40. S.A. Shehzad, T. Hayat, M. Qasim, S. Asghar, Braz. J. Chem. Eng. **30**, 187 (2013).
41. S.A. Shehzad, M. Qasim, A. Alsaedi, T. Hayat, M.S. Alhuthali, Eur. Phys. J. Plus **128**, 7 (2013).
42. T. Hayat, S.A. Shehzad, S. Asghar, Walailak J. Sci. Technol. **10**, 29 (2013).
43. M. Sheikholeslami, M. Gorji-Bandpay, D.D. Ganji, Arabian J. Sci. Eng. **39**, 5007 (2014).
44. M. Sheikholeslami, D.D. Ganji, J. Appl. Fluid Mech. **7**, 535 (2014).
45. Mohsen Sheikholeslami, Mofid Gorji Bandpy, R. Ellahi, A. Zeeshan, J. Magn. Magn. Mat. **369**, 69 (2014).
46. M. Sheikholeslami, M. Gorji-Bandpy, D.D. Ganji, J. Taiwan Inst. Chem. Eng. **45**, 1204 (2014).
47. M. Sheikholeslami, D.D. Ganji, Sci. Iran. B **21**, 203 (2014).
48. T. Hayat, S.A. Shehzad, A. Alsaedi, M.S. Alhuthali, Appl. Math. Mech. **34**, 489 (2013).
49. T. Hayat, M. Waqas, S.A. Shehzad, A. Alsaedi, J. Mech. **29**, 403 (2013).
50. S.A. Shehzad, F.E. Alsaadi, S.J. Monaquel, T. Hayat, Eur. Phys. J. Plus **128**, 56 (2013).
51. T. Hayat, S.A. Shehzad, M. Qasim, S. Asghar, A. Alsaedi, J. Thermophys. Heat Transfer **28**, 155 (2014).
52. T. Hayat, S.A. Shehzad, M. Qasim, S. Asghar, Int. J. Numer. Methods Heat Fluid Flow **24**, 342 (2014).
53. M. Sheikholeslami, D.D. Ganji, J. Mol. Liq. **194**, 13 (2014).
54. M. Sheikholeslami, M. Gorji-Bandpy, D.D. Ganji, Powder Technol. **254**, 82 (2014).
55. M. Sheikholeslami, D.D. Ganji, Powder Technol. **253**, 789 (2014).
56. T. Hayat, S.A. Shehzad, M. Qasim, A. Alsaedi, Braz. J. Chem. Eng. **31**, 109 (2014).
57. S.A. Shehzad, A. Alsaedi, T. Hayat, M.S. Alhuthali, J. Taiwan Inst. Chem. Eng. **45**, 787 (2014).
58. S.A. Shehzad, T. Hayat, M.S. Alhuthali, S. Asghar, J. Cent. South Univ. **21**, 1428 (2014).
59. T. Hayat, S.A. Shehzad, S. Al-Mezel, A. Alsaedi, J. Hydrol. Hydromech. **62**, 117 (2014).
60. M. Sheikholeslami, M. Gorji-Bandpy, D.D. Ganji, Energy **60**, 501 (2013).
61. M. Sheikholeslami, D.D. Ganji, M. Gorji-Bandpy, Soheil Soleimani, J. Taiwan Inst. Chem. Eng. **45**, 795 (2014).
62. M. Sheikholeslami, D.D. Ganji, Houman B. Rokni, Int. J. Eng. Trans. C **26**, 653 (2013).
63. V. Loukopoulos, E. Tzirtzilakis, Int. J. Eng. Sci. **42**, 571 (2004).
64. H. Aminfar, M. Mohammadpourfard, F. Mohseni, J. Magn. Magn. Mater. **324**, 830 (2012).
65. K. Khanafer, K. Vafai, M. Lightstone, Int. J. Heat Mass Transfer **46**, 3639 (2003).
66. G. De Vahl Davis, Int. J. Numer. Methods Fluids **3**, 249 (1962).